J|A|C|S COMMUNICATIONS

Published on Web 07/31/2009

Synthesis of Cu_2ZnSnS_4 Nanocrystal Ink and Its Use for Solar Cells

Qijie Guo, Hugh W. Hillhouse,* and Rakesh Agrawal*

School of Chemical Engineering and the Energy Center, Purdue University, West Lafayette, Indiana 47906

Received June 17, 2009; E-mail: agrawalr@purdue.edu; hugh@purdue.edu

Advances in the colloidal synthesis of high quality nanocrystals have opened up new possible routes to address the challenge of fabricating low-cost, high-efficiency solar cells.[1] In particular, photovoltaic devices based on several semiconductor nanocrystals have recently been demonstrated, including Cu_2S,[2] CdTe,[3] PbSe,[4] $Pb(S_x,Se_{1-x})$,[5] $CuInSe_2$, $Cu(In,Ga)Se_2$,[6−8] and $Cu(In_{1-x},Ga_x)S_2$.[9] In one approach, the semiconductor nanocrystals can be used in the form of a nanocrystal ink that is coated on a substrate and sintered into bulk material to yield a low-cost solar cell fabrication process.

Among the various semiconductor nanocrystals, one of the most promising candidates for low cost thin film photovoltaics is the I−III−VI_2 family of chalcogenide nanocrystals. However, due to the limited supply and increasing price of rare metals, such as indium and gallium, there is a need to find alternative materials with high abundance and low cost. Recently, there has been an effort to investigate direct band gap Cu_2ZnSnS_4[10] (CZTS) and $Cu_2ZnSnSe_4$ (CZTSe) thin films for photovoltaic applications. CZTS and CZTSe are particularly attractive because Sn and Zn are naturally abundant in the Earth's crust and have relatively low toxicity. Solar cells based on CZTS have achieved power conversion efficiencies as high as 6.77% under AM1.5G illumination.[11] However, Shockley−Queisser photon balance calculations show that the theoretical limit for CZTS is 32.2%. Various high-vacuum and nonvacuum based techniques similar to those explored for $Cu(In,Ga)Se_2$ absorbers have been investigated for the deposition of CZTS thin films including coevaporation and selenization of various precursor layers.[12−17] Here, we report the first synthesis of I_2−II−IV−VI_4 nanocrystals of Cu_2ZnSnS_4 and demonstrate their use in the fabrication of solar cells.

CZTS nanocrystals are synthesized by hot injection of a solution of elemental sulfur in oleylamine into an oleylamine solution containing 1.5 mmol of copper(II) acetylacetonate, 0.75 mmol of zinc acetylacetonate, and 0.75 mmol of tin(IV) bis(acetylacetonate) dibromide at 225 °C. Please refer to the Supporting Information for experimental details. Figure 1 shows the PXRD pattern of the as-synthesized CZTS nanocrystals. CZTS is a tetrahedrally coordinated semiconductor where each sulfur anion is bonded to four cations and each cation is bonded to four sulfur anions. The ordering of the cations in the cation sublattice may occur in at least two variations. In one (the stannite structure), cation layers alternate with sulfur anion layers along the crystallographic *c*-direction as CuCu/SS/ZnSn/SS. In another (the kesterite structure), the cation and anion layers alternate as CuZn/SS/CuSn/SS. Both variations are described by tetragonal unit cells. Note these are both similar to the chalcopyrite structure such as $CuInS_2$ where cation and anion layers alternate as CuIn/SS/CuIn/SS. The kesterite and stannite powder X-ray diffraction (PXRD) patterns differ only slightly in the splitting of high order peaks, such as (220)/(204) and (116)/(312) due to a slightly different tetragonal distortion (c/2a). However, here the structure cannot be distinguished between kesterite and stannite using PXRD due to peak broadening, and the PXRD pattern of the as-synthesized CZTS nanocrystals (Figure 1a) agrees well with either the kesterite (simulated PXRD pattern shown in Figure 1) or stannite (PDF #26-0575) diffraction patterns. Though, on the basis of first principle calculations, kesterite has been reported to be more thermodynamically stable than stannite.[18,19] The lattice parameters calculated for the CZTS nanocrystals based on the (220) and (112) PXRD peaks are 5.421 and 10.816 Å for *a* and *c* respectively. The crystal domain size estimated from fwhm of the (112) peak by the Scherrer equation is 16 nm.

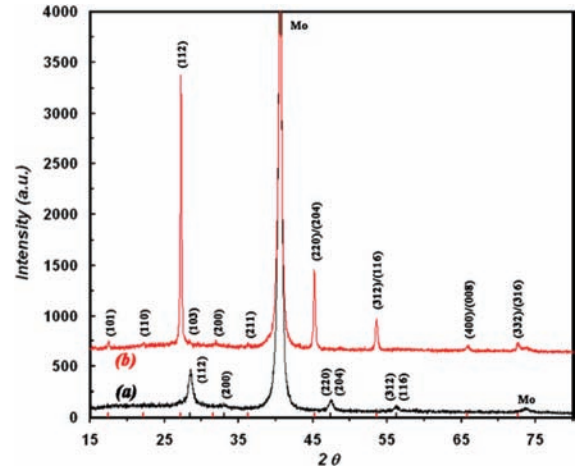

Figure 1. PXRD patterns of (a) as-synthesized CZTS nanocrystals coated on a Mo coated soda lime glass and (b) after annealing under a Se atmosphere at 500 °C for 20 min. Diffraction peaks of the selenized films shift systematically to the left due to the increase in lattice parameter with Se replacing S in the CZTS matrix. The simulated peak positions using experimentally determined lattice parameters with the kesterite crystal structure are indicated by the black and red tick marks for CZTS and CZTSSe, respectively.

Figure 2a shows a transmission electron microscopy (TEM) image of the as-synthesized CZTS nanocrystals. The CZTS nanocrystals are slightly polydispersed with most of the nanocrystals falling in the range 15−25 nm. The average size of the CZTS nanocrystals corresponds well with the crystalline size estimated from PXRD. The absorption spectrum of the as-synthesized CZTS nanocrystals is measured using UV−vis absorbance spectroscopy, Figure 2b. The band gap of the CZTS nanocrystals is estimated to be 1.5 eV by extrapolating the linear region of a plot of the absorbance squared versus energy as shown in the inset of Figure 2b. The observed band gap corresponds well with that reported in the literature (1.45−1.51 eV).[20,21] The average composition of the CZTS nanocrystals is determined using EDX to be $Cu_{2.12}Zn_{0.84}Sn_{1.06}S_4$, which is slightly copper rich with a Zn/Sn ratio of 0.79. This composition is within the range of compositions reported for CZTS films by several researchers.[14−19]

For the fabrication of nanocrystal-ink-based solar cells, the suspended CZTS nanocrystals are applied directly to Mo (500 nm) coated soda lime glass substrates by drop-casting to form nano-

10.1021/ja904981r CCC: $40.75

crystal thin films. The CZTS nanocrystal films are then selenized to form $Cu_2ZnSnS_ySe_{1-y}$ (referred to as CZTSSe) absorbers by annealing under Se vapor in a graphite box at temperatures between 400 and 500 °C. The PXRD pattern of a CZTSSe film selenized at 500 °C for 20 min is shown in Figure 1. After selenization, the diffraction peaks shift to the left systematically due to expansion in the unit cell volume with the replacement of S by Se. The unit cell remains tetragonal, and the lattice parameters *a* and *c* shift to 5.667 and 11.296 Å, respectively. Also, the X-ray diffraction peaks sharpen, indicating growth of the crystalline domain size. In addition, other minor peaks such as (101) and (211) become observable. The amount of sulfur in the selenized CZTSSe film is typically 5−6% as determined by EDX on an equivalent sample prepared on a bare soda lime glass substrate since the Mo Lα peak overlaps with the S Kα peak.

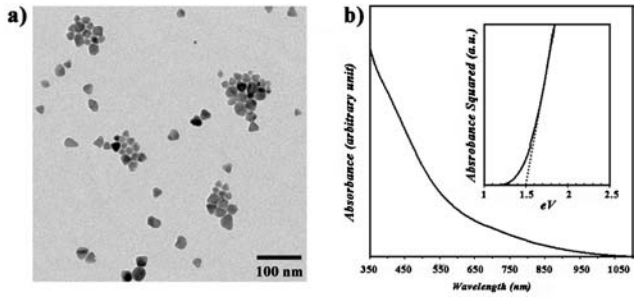

Figure 2. (a) TEM image and (b) UV−vis absorption spectrum of the as-synthesized CZTS nanocrystals. Inset of Figure 2b shows the abs^2 vs eV for the CZTS nanocrystals; the estimated band gap energy is 1.5 eV.

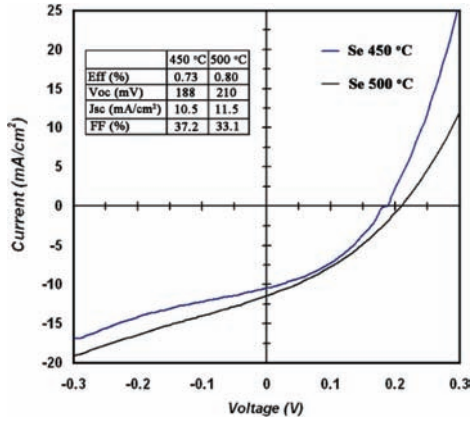

Figure 3. *I*−*V* characteristics of initial CZTSSe photovoltaic devices fabricated using CZTS nanocrystals films selenized at 450 and 500 °C. The reported efficiencies are based on nonshadowed areas under AM1.5G illumination.

The CZTSSe absorber films are then processed into photovoltaic devices by chemical bath deposition of CdS (50 nm), RF sputtering of *i*-ZnO (50 nm), and RF sputtering of ITO (250 nm). The final devices are scribed into small areas of 0.12 cm^2 with a small dap of silver paint applied to form the top contact. Figure 3 shows the current−voltage (*I*−*V*) characteristics for devices fabricated using CZTS nanocrystal films selenized at temperatures of 450 and 500 °C, respectively. The absorber film selenized at 500 °C has a slightly higher Voc and Jsc as compared to the film selenized at 450 °C. Initial devices fabricated using the CZTSSe films show a power conversion efficiency of 0.74% which corresponds to 0.80% based on the nonshadowed area under AM1.5G illumination. The device efficiencies are low primarily due to low open circuit voltages and fill factor, likely a result of the slightly copper-rich composition in the film. Based on *I*−*V* characteristics derived from a photon balance (similar to that used by Shockley and Queisser), the ideal device parameters for a single junction CZTS solar cell under AM1.5G are as follows: open circuit voltage of 1.23 V, short-circuit current of 29.0 mA/cm^2, fill factor of 90.0%, and a power conversion efficiency of 32.2%.

In conclusion, a facile synthesis for quaternary CZTS nanocrystals has been reported for the first time. CZTS nanocrystals and selenized CZTSSe films have suitable optical properties for efficient solar energy conversion and can be utilized for the preparation of functioning photovoltaic devices. Initial photovoltaic devices fabricated using the CZTSSe absorber films showed device efficiencies up to 0.74% which corresponds to 0.80% based on the nonshadowed area under AM1.5G illumination. Improvements in device performance are expected with further studies as more of the material properties of CZTS nanocrystals and CZTSSe absorber films are understood.

Supporting Information Available: Experimental details on synthesis of CZTS nanocrystals, device fabrication and analysis. This materials is available free of charge via the Internet at http://pubs.acs.org.

References

(1) Hillhouse, H. W.; Beard, M. C. *Colloid Interface Sci.* **2009**, *14*, 245–259.
(2) Scragg, J. J.; Dale, P. J.; Peter, L. M. *Thin Solid Films* **2009**, *517*, 2481–2484.
(3) Gur, I.; Fromer, N. A.; Geier, M. L.; Alivisatos, A. P. *Science* **2005**, *310*, 462–465.
(4) Luther, J. M.; Law, M.; Beard, M. C.; Song, Q.; Reese, M. O.; Ellingson, R. J.; Nozik, A. J. *Nano Lett.* **2008**, *8*, 3488–3492.
(5) Ma, W.; Luther, J. M.; Zheng, H. M.; Wu, Y.; Alivisatos, A. P. *Nano Lett.* **2009**, *9*, 1699–1703.
(6) Guo, Q.; Agrawal, R.; Hillhouse, H. Rapid synthesis of ternary, binary and multinary chalcogenide nanoparticles. International Patent Application No. PCT/US2007/069349, 2007.
(7) Guo, Q.; Kim, S. J.; Kar, M.; Shafarman, W. N.; Birkmire, R. W.; Stach, E. A.; Agrawal, R.; Hillhouse, H. W. *Nano Lett.* **2008**, *8*, 2982–2987.
(8) Panthani, M. G.; Akhavan, V.; Goodfellow, B.; Schmidtke, J. P.; Dunn, L.; Dodabalapur, A.; Barbara, P. F.; Korgel, B. A. *J. Am. Chem. Soc.* **2008**, *130*, 16770–16777.
(9) Guo, Q.; Ford, G. M.; Hillhouse, H. W.; Agrawal, R. *Nano Lett.* **2009** (ASAP).
(10) Katagiri, H.; Ishigaki, N.; Ishida, T.; Saito, K. *Jpn. J. Appl. Phys., Part 1* **2001**, *40*, 500–504.
(11) Katagiri, H.; Jimbo, K.; Maw, W. S.; Oishi, K.; Yamazaki, M.; Araki, H.; Takeuchi, A. *Thin Solid Films* **2009**, *517*, 2455–2460.
(12) Araki, H.; Mikaduki, A.; Kubo, Y.; Sato, T.; Jimbo, K.; Maw, W. S.; Katagiri, H.; Yamazaki, M.; Oishi, K.; Takeuchi, A. *Thin Solid Films* **2008**, *517*, 1457–1460.
(13) Ennaoui, A.; Lux-Steiner, M.; Weber, A.; Abou-Ras, D.; Kotschau, I.; Schock, H. W.; Schurr, R.; Holzing, A.; Jost, S.; Hock, R.; Voss, T.; Schulze, J.; Kirbs, A. *Thin Solid Films* **2009**, *517*, 2511–2514.
(14) Katagiri, H.; Sasaguchi, N.; Hando, S.; Hoshino, S.; Ohashi, J.; Yokota, T. *Sol. Energy Mater. Sol. Cells* **1997**, *49*, 407–414.
(15) Tanaka, T.; Kawasaki, D.; Nishio, M.; Gu, Q. X.; Ogawal, H. *Phys. Status Solidi B* **2006**, *3*, 2844–2847.
(16) Tanaka, K.; Moritake, N.; Uchiki, H. *Sol. Energy Mater. Sol. Cells* **2007**, *91*, 1199–1201.
(17) Weber, A.; Krauth, H.; Perlt, S.; Schubert, B.; Kotschau, I.; Schorr, S.; Schock, H. W. *Thin Solid Films* **2009**, *517*, 2524–2526.
(18) Chen, S. Y.; Gong, X. G.; Walsh, A.; Wei, S. H. *Phys. Rev. B* **2009**, *79*, 165211.
(19) Paier, J.; Asahi, R.; Nagoya, A.; Kresse, G. *Phys. Rev. B* **2009**, *79*, 115126.
(20) Ito, K.; Nakazawa, T. *Jpn. J. Appl. Phys., Part 1* **1988**, *27*, 2094–2097.
(21) Katagiri, H. *Thin Solid Films* **2005**, *480*, 426–432.

JA904981R